Fermilab-Pub-12/020-E

Measurement of the Top Quark Mass in $p\bar{p}$ Collisions using Events with Two Leptons

V.M. Abazov,[34] B. Abbott,[72] B.S. Acharya,[28] M. Adams,[48] T. Adams,[46] G.D. Alexeev,[34] G. Alkhazov,[38] A. Alton[a],[60] G. Alverson,[59] M. Aoki,[47] A. Askew,[46] B. Åsman,[40] S. Atkins,[57] O. Atramentov,[64] K. Augsten,[9] C. Avila,[7] J. BackusMayes,[79] F. Badaud,[12] L. Bagby,[47] B. Baldin,[47] D.V. Bandurin,[46] S. Banerjee,[28] E. Barberis,[59] P. Baringer,[55] J. Barreto,[3] J.F. Bartlett,[47] U. Bassler,[17] V. Bazterra,[48] A. Bean,[55] M. Begalli,[3] C. Belanger-Champagne,[40] L. Bellantoni,[47] S.B. Beri,[26] G. Bernardi,[16] R. Bernhard,[21] I. Bertram,[41] M. Besançon,[17] R. Beuselinck,[42] V.A. Bezzubov,[37] P.C. Bhat,[47] S. Bhatia,[62] V. Bhatnagar,[26] G. Blazey,[49] S. Blessing,[46] K. Bloom,[63] A. Boehnlein,[47] D. Boline,[69] E.E. Boos,[36] G. Borissov,[41] T. Bose,[58] A. Brandt,[75] O. Brandt,[22] R. Brock,[61] G. Brooijmans,[67] A. Bross,[47] D. Brown,[16] J. Brown,[16] X.B. Bu,[47] M. Buehler,[47] V. Buescher,[23] V. Bunichev,[36] S. Burdin[b],[41] T.H. Burnett,[79] C.P. Buszello,[40] B. Calpas,[14] E. Camacho-Pérez,[31] M.A. Carrasco-Lizarraga,[55] B.C.K. Casey,[47] H. Castilla-Valdez,[31] S. Chakrabarti,[69] D. Chakraborty,[49] K.M. Chan,[53] A. Chandra,[77] E. Chapon,[17] G. Chen,[55] S. Chevalier-Théry,[17] D.K. Cho,[74] S.W. Cho,[30] S. Choi,[30] B. Choudhary,[27] S. Cihangir,[47] D. Claes,[63] J. Clutter,[55] M. Cooke,[47] W.E. Cooper,[47] M. Corcoran,[77] F. Couderc,[17] M.-C. Cousinou,[14] A. Croc,[17] D. Cutts,[74] A. Das,[44] G. Davies,[42] S.J. de Jong,[33] E. De La Cruz-Burelo,[31] F. Déliot,[17] R. Demina,[68] D. Denisov,[47] S.P. Denisov,[37] S. Desai,[47] C. Deterre,[17] K. DeVaughan,[63] H.T. Diehl,[47] M. Diesburg,[47] P.F. Ding,[43] A. Dominguez,[63] T. Dorland,[79] A. Dubey,[27] L.V. Dudko,[36] D. Duggan,[64] A. Duperrin,[14] S. Dutt,[26] A. Dyshkant,[49] M. Eads,[63] D. Edmunds,[61] J. Ellison,[45] V.D. Elvira,[47] Y. Enari,[16] H. Evans,[51] A. Evdokimov,[70] V.N. Evdokimov,[37] G. Facini,[59] T. Ferbel,[68] F. Fiedler,[23] F. Filthaut,[33] W. Fisher,[61] H.E. Fisk,[47] M. Fortner,[49] H. Fox,[41] S. Fuess,[47] A. Garcia-Bellido,[68] G.A. García-Guerra[c],[31] V. Gavrilov,[35] P. Gay,[12] W. Geng,[14,61] D. Gerbaudo,[65] C.E. Gerber,[48] Y. Gershtein,[64] G. Ginther,[47,68] G. Golovanov,[34] A. Goussiou,[79] P.D. Grannis,[69] S. Greder,[18] H. Greenlee,[47] Z.D. Greenwood,[57] E.M. Gregores,[4] G. Grenier,[19] Ph. Gris,[12] J.-F. Grivaz,[15] A. Grohsjean[d],[17] S. Grünendahl,[47] M.W. Grünewald,[29] T. Guillemin,[15] G. Gutierrez,[47] P. Gutierrez,[72] A. Haas[e],[67] S. Hagopian,[46] J. Haley,[59] L. Han,[6] K. Harder,[43] A. Harel,[68] J.M. Hauptman,[54] J. Hays,[42] T. Head,[43] T. Hebbeker,[20] D. Hedin,[49] H. Hegab,[73] A.P. Heinson,[45] U. Heintz,[74] C. Hensel,[22] I. Heredia-De La Cruz,[31] K. Herner,[60] G. Hesketh[f],[43] M.D. Hildreth,[53] R. Hirosky,[78] T. Hoang,[46] J.D. Hobbs,[69] B. Hoeneisen,[11] M. Hohlfeld,[23] Z. Hubacek,[9,17] V. Hynek,[9] I. Iashvili,[66] Y. Ilchenko,[76] R. Illingworth,[47] A.S. Ito,[47] S. Jabeen,[74] M. Jaffré,[15] D. Jamin,[14] A. Jayasinghe,[72] R. Jesik,[42] K. Johns,[44] M. Johnson,[47] A. Jonckheere,[47] P. Jonsson,[42] J. Joshi,[26] A.W. Jung,[47] A. Juste,[39] K. Kaadze,[56] E. Kajfasz,[14] D. Karmanov,[36] P.A. Kasper,[47] I. Katsanos,[63] R. Kehoe,[76] S. Kermiche,[14] N. Khalatyan,[47] A. Khanov,[73] A. Kharchilava,[66] Y.N. Kharzheev,[34] J.M. Kohli,[26] A.V. Kozelov,[37] J. Kraus,[61] S. Kulikov,[37] A. Kumar,[66] A. Kupco,[10] T. Kurča,[19] V.A. Kuzmin,[36] S. Lammers,[51] G. Landsberg,[74] P. Lebrun,[19] H.S. Lee,[30] S.W. Lee,[54] W.M. Lee,[47] J. Lellouch,[16] H. Li,[13] L. Li,[45] Q.Z. Li,[47] S.M. Lietti,[5] J.K. Lim,[30] D. Lincoln,[47] J. Linnemann,[61] V.V. Lipaev,[37] R. Lipton,[47] H. Liu,[76] Y. Liu,[6] A. Lobodenko,[38] M. Lokajicek,[10] R. Lopes de Sa,[69] H.J. Lubatti,[79] R. Luna-Garcia[g],[31] A.L. Lyon,[47] A.K.A. Maciel,[2] D. Mackin,[77] R. Madar,[17] R. Magaña-Villalba,[31] S. Malik,[63] V.L. Malyshev,[34] Y. Maravin,[56] J. Martínez-Ortega,[31] R. McCarthy,[69] C.L. McGivern,[55] M.M. Meijer,[33] A. Melnitchouk,[62] D. Menezes,[49] P.G. Mercadante,[4] M. Merkin,[36] A. Meyer,[20] J. Meyer,[22] F. Miconi,[18] N.K. Mondal,[28] G.S. Muanza,[14] M. Mulhearn,[78] E. Nagy,[14] M. Naimuddin,[27] M. Narain,[74] R. Nayyar,[27] H.A. Neal,[60] J.P. Negret,[7] P. Neustroev,[38] S.F. Novaes,[5] T. Nunnemann,[24] G. Obrant[‡],[38] J. Orduna,[77] N. Osman,[14] J. Osta,[53] G.J. Otero y Garzón,[1] M. Padilla,[45] A. Pal,[75] N. Parashar,[52] V. Parihar,[74] S.K. Park,[30] R. Partridge[e],[74] N. Parua,[51] A. Patwa,[70] B. Penning,[47] M. Perfilov,[36] Y. Peters,[43] K. Petridis,[43] G. Petrillo,[68] P. Pétroff,[15] R. Piegaia,[1] M.-A. Pleier,[70] P.L.M. Podesta-Lerma[h],[31] V.M. Podstavkov,[47] P. Polozov,[35] A.V. Popov,[37] M. Prewitt,[77] D. Price,[51] N. Prokopenko,[37] J. Qian,[60] A. Quadt,[22] B. Quinn,[62] M.S. Rangel,[2] K. Ranjan,[27] P.N. Ratoff,[41] I. Razumov,[37] P. Renkel,[76] M. Rijssenbeek,[69] I. Ripp-Baudot,[18] F. Rizatdinova,[73] M. Rominsky,[47] A. Ross,[41] C. Royon,[17] P. Rubinov,[47] R. Ruchti,[53] G. Safronov,[35] G. Sajot,[13] P. Salcido,[49] A. Sánchez-Hernández,[31] M.P. Sanders,[24] B. Sanghi,[47] A.S. Santos,[5] G. Savage,[47] L. Sawyer,[57] T. Scanlon,[42] R.D. Schamberger,[69] Y. Scheglov,[38] H. Schellman,[50] T. Schliephake,[25] S. Schlobohm,[79] C. Schwanenberger,[43] R. Schwienhorst,[61] J. Sekaric,[55] H. Severini,[72] E. Shabalina,[22] V. Shary,[17] A.A. Shchukin,[37] R.K. Shivpuri,[27] V. Simak,[9] V. Sirotenko,[47] P. Skubic,[72] P. Slattery,[68] D. Smirnov,[53] K.J. Smith,[66] G.R. Snow,[63] J. Snow,[71] S. Snyder,[70] S. Söldner-Rembold,[43] L. Sonnenschein,[20] K. Soustruznik,[8] J. Stark,[13] V. Stolin,[35] D.A. Stoyanova,[37] M. Strauss,[72] D. Strom,[48] L. Stutte,[47] L. Suter,[43] P. Svoisky,[72] M. Takahashi,[43] A. Tanasijczuk,[1] M. Titov,[17] V.V. Tokmenin,[34] Y.-T. Tsai,[68] K. Tschann-Grimm,[69] D. Tsybychev,[69] B. Tuchming,[17] C. Tully,[65] L. Uvarov,[38]

S. Uvarov,[38] S. Uzunyan,[49] R. Van Kooten,[51] W.M. van Leeuwen,[32] N. Varelas,[48] E.W. Varnes,[44] I.A. Vasilyev,[37] P. Verdier,[19] L.S. Vertogradov,[34] M. Verzocchi,[47] M. Vesterinen,[43] D. Vilanova,[17] P. Vokac,[9] H.D. Wahl,[46] M.H.L.S. Wang,[47] J. Warchol,[53] G. Watts,[79] M. Wayne,[53] M. Weber[i],[47] J. Weichert,[23] L. Welty-Rieger,[50] A. White,[75] D. Wicke,[25] M.R.J. Williams,[41] G.W. Wilson,[55] M. Wobisch,[57] D.R. Wood,[59] T.R. Wyatt,[43] Y. Xie,[47] R. Yamada,[47] W.-C. Yang,[43] T. Yasuda,[47] Y.A. Yatsunenko,[34] W. Ye,[69] Z. Ye,[47] H. Yin,[47] K. Yip,[70] S.W. Youn,[47] T. Zhao,[79] B. Zhou,[60] J. Zhu,[60] M. Zielinski,[68] D. Zieminska,[51] and L. Zivkovic[74]

(The D0 Collaboration)*

[1]*Universidad de Buenos Aires, Buenos Aires, Argentina*
[2]*LAFEX, Centro Brasileiro de Pesquisas Físicas, Rio de Janeiro, Brazil*
[3]*Universidade do Estado do Rio de Janeiro, Rio de Janeiro, Brazil*
[4]*Universidade Federal do ABC, Santo André, Brazil*
[5]*Instituto de Física Teórica, Universidade Estadual Paulista, São Paulo, Brazil*
[6]*University of Science and Technology of China, Hefei, People's Republic of China*
[7]*Universidad de los Andes, Bogotá, Colombia*
[8]*Charles University, Faculty of Mathematics and Physics, Center for Particle Physics, Prague, Czech Republic*
[9]*Czech Technical University in Prague, Prague, Czech Republic*
[10]*Center for Particle Physics, Institute of Physics, Academy of Sciences of the Czech Republic, Prague, Czech Republic*
[11]*Universidad San Francisco de Quito, Quito, Ecuador*
[12]*LPC, Université Blaise Pascal, CNRS/IN2P3, Clermont, France*
[13]*LPSC, Université Joseph Fourier Grenoble 1, CNRS/IN2P3, Institut National Polytechnique de Grenoble, Grenoble, France*
[14]*CPPM, Aix-Marseille Université, CNRS/IN2P3, Marseille, France*
[15]*LAL, Université Paris-Sud, CNRS/IN2P3, Orsay, France*
[16]*LPNHE, Universités Paris VI and VII, CNRS/IN2P3, Paris, France*
[17]*CEA, Irfu, SPP, Saclay, France*
[18]*IPHC, Université de Strasbourg, CNRS/IN2P3, Strasbourg, France*
[19]*IPNL, Université Lyon 1, CNRS/IN2P3, Villeurbanne, France and Université de Lyon, Lyon, France*
[20]*III. Physikalisches Institut A, RWTH Aachen University, Aachen, Germany*
[21]*Physikalisches Institut, Universität Freiburg, Freiburg, Germany*
[22]*II. Physikalisches Institut, Georg-August-Universität Göttingen, Göttingen, Germany*
[23]*Institut für Physik, Universität Mainz, Mainz, Germany*
[24]*Ludwig-Maximilians-Universität München, München, Germany*
[25]*Fachbereich Physik, Bergische Universität Wuppertal, Wuppertal, Germany*
[26]*Panjab University, Chandigarh, India*
[27]*Delhi University, Delhi, India*
[28]*Tata Institute of Fundamental Research, Mumbai, India*
[29]*University College Dublin, Dublin, Ireland*
[30]*Korea Detector Laboratory, Korea University, Seoul, Korea*
[31]*CINVESTAV, Mexico City, Mexico*
[32]*Nikhef, Science Park, Amsterdam, the Netherlands*
[33]*Radboud University Nijmegen, Nijmegen, the Netherlands and Nikhef, Science Park, Amsterdam, the Netherlands*
[34]*Joint Institute for Nuclear Research, Dubna, Russia*
[35]*Institute for Theoretical and Experimental Physics, Moscow, Russia*
[36]*Moscow State University, Moscow, Russia*
[37]*Institute for High Energy Physics, Protvino, Russia*
[38]*Petersburg Nuclear Physics Institute, St. Petersburg, Russia*
[39]*Institució Catalana de Recerca i Estudis Avançats (ICREA) and Institut de Física d'Altes Energies (IFAE), Barcelona, Spain*
[40]*Stockholm University, Stockholm and Uppsala University, Uppsala, Sweden*
[41]*Lancaster University, Lancaster LA1 4YB, United Kingdom*
[42]*Imperial College London, London SW7 2AZ, United Kingdom*
[43]*The University of Manchester, Manchester M13 9PL, United Kingdom*
[44]*University of Arizona, Tucson, Arizona 85721, USA*
[45]*University of California Riverside, Riverside, California 92521, USA*
[46]*Florida State University, Tallahassee, Florida 32306, USA*
[47]*Fermi National Accelerator Laboratory, Batavia, Illinois 60510, USA*
[48]*University of Illinois at Chicago, Chicago, Illinois 60607, USA*
[49]*Northern Illinois University, DeKalb, Illinois 60115, USA*
[50]*Northwestern University, Evanston, Illinois 60208, USA*
[51]*Indiana University, Bloomington, Indiana 47405, USA*
[52]*Purdue University Calumet, Hammond, Indiana 46323, USA*

[53] University of Notre Dame, Notre Dame, Indiana 46556, USA
[54] Iowa State University, Ames, Iowa 50011, USA
[55] University of Kansas, Lawrence, Kansas 66045, USA
[56] Kansas State University, Manhattan, Kansas 66506, USA
[57] Louisiana Tech University, Ruston, Louisiana 71272, USA
[58] Boston University, Boston, Massachusetts 02215, USA
[59] Northeastern University, Boston, Massachusetts 02115, USA
[60] University of Michigan, Ann Arbor, Michigan 48109, USA
[61] Michigan State University, East Lansing, Michigan 48824, USA
[62] University of Mississippi, University, Mississippi 38677, USA
[63] University of Nebraska, Lincoln, Nebraska 68588, USA
[64] Rutgers University, Piscataway, New Jersey 08855, USA
[65] Princeton University, Princeton, New Jersey 08544, USA
[66] State University of New York, Buffalo, New York 14260, USA
[67] Columbia University, New York, New York 10027, USA
[68] University of Rochester, Rochester, New York 14627, USA
[69] State University of New York, Stony Brook, New York 11794, USA
[70] Brookhaven National Laboratory, Upton, New York 11973, USA
[71] Langston University, Langston, Oklahoma 73050, USA
[72] University of Oklahoma, Norman, Oklahoma 73019, USA
[73] Oklahoma State University, Stillwater, Oklahoma 74078, USA
[74] Brown University, Providence, Rhode Island 02912, USA
[75] University of Texas, Arlington, Texas 76019, USA
[76] Southern Methodist University, Dallas, Texas 75275, USA
[77] Rice University, Houston, Texas 77005, USA
[78] University of Virginia, Charlottesville, Virginia 22901, USA
[79] University of Washington, Seattle, Washington 98195, USA

(Dated: January 24, 2012)

We present a measurement of the top-quark mass (m_t) in $p\bar{p}$ collisions at $\sqrt{s} = 1.96$ TeV using $t\bar{t}$ events with two leptons (ee, $e\mu$, or $\mu\mu$) and accompanying jets in 4.3 fb^{-1} of data collected with the D0 detector at the Fermilab Tevatron collider. We analyze the kinematically underconstrained dilepton events by integrating over their neutrino rapidity distributions. We reduce the dominant systematic uncertainties from the calibration of jet energy using a correction obtained from $t\bar{t}$ events with a final state of a single lepton plus jets. We also correct jets in simulated events to replicate the quark flavor dependence of the jet response in data. We measure $m_t = 173.7 \pm 2.8\,(\text{stat}) \pm 1.5\,(\text{syst})$ GeV and combining with our analysis in 1 fb^{-1} of preceding data we measure $m_t = 174.0 \pm 2.4\,(\text{stat}) \pm 1.4\,(\text{syst})$ GeV. Taking into account statistical and systematic correlations, a combination with the D0 matrix element result from both data sets yields $m_t = 173.9 \pm 1.9\,(\text{stat}) \pm 1.6\,(\text{syst})$ GeV.

PACS numbers: 12.15.Ff, 14.65.Ha

The masses of fundamental fermions in the standard model (SM) are generated through their interaction with a hypothesized scalar Higgs field with a strength given by a Yukawa coupling specific to each fermion species. The Yukawa coupling of the top quark corresponds to unity within uncertainties, and this value is constrained by a measurement of the top-quark mass (m_t). In direct searches at the LHC for the standard model Higgs boson, both the CMS and ATLAS experiments observe local excesses above the background expectations for a Higgs boson mass (m_H) of approximately 125 GeV/c^2 [1, 2], decaying to diboson final states. Combined results in searches from the CDF and D0 experiments at the Tevatron show evidence for events above background expectation in $b\bar{b}$ final states [3]. It is therefore important to sharpen the measurement of m_t, as its precise value, along with the mass of the W boson (m_W), constrain the standard model prediction for m_H through well defined radiative corrections.

In $p\bar{p}$ collisions, top quarks (t) are primarily produced in $t\bar{t}$ pairs, with each top quark decaying with $BR(t \to Wb) \sim 100\%$. These events yield final states with either 0, 1, or 2 leptons from decays of the two W bosons. We consider the dilepton channels (2ℓ) that contain either electrons or muons of large transverse momentum (p_T) and at least two jets. We analyzed such events previously [4, 5] using the neutrino-weighting (νWT) approach [6]. While the 2ℓ channels have low background, the small decay branching ratio into leptons means that

---

* with visitors from [a]Augustana College, Sioux Falls, SD, USA, [b]The University of Liverpool, Liverpool, UK, [c]UPIITA-IPN, Mexico City, Mexico, [d]DESY, Hamburg, Germany, [e]SLAC, Menlo Park, CA, USA, [f]University College London, London, UK, [g]Centro de Investigacion en Computacion - IPN, Mexico City, Mexico, [h]ECFM, Universidad Autonoma de Sinaloa, Culiacán, Mexico, and [i]Universität Bern, Bern, Switzerland. [‡]Deceased.

m_t measurements from these events remained statistically limited unlike in channels with one lepton and four or more jets (ℓ+jets). This situation has changed recently (e.g., Ref. [7]). Now, dominant systematic uncertainties from jet energy calibration, which have been larger [4] in the dilepton channel compared to ℓ+jets, are limiting precision of the m_t measurement. In ℓ+jets events, two quarks originate from W boson decay and yield a dijet mass signature that permits a precise calibration of jet energies for the measurement of m_t in $t\bar{t}$ events [8]. While this calibration has greatly improved measurements in the ℓ+jets channels, it has not been carried over to the calibration in other analyses. This is primarily due to differences in event topologies that can affect the details of the jet energy scale.

We present a new measurement of m_t using the D0 detector with 4.3 fb^{-1} of $p\bar{p}$ collider data in the ee, $e\mu$, and $\mu\mu$ final states. We improve the jet energy calibration for the accompanying jets using the energy scale from ℓ+jets events [10]. Our approach differs from that of Ref. [11] in that we do not use the ℓ+jets scale as a constraint in a combined fit of ℓ+jets and dilepton events. Instead, we use this constraint as a calibration, and estimate the uncertainties of transferring that calibration to the dilepton event topology. This procedure demonstrates how the calibration obtained using the dijet constraint from m_W can be applied to different final states, and has wide applicability beyond the measurement of m_t in 2ℓ events. We also employ flavor-dependent corrections to jet energies for the first time in a dilepton analysis that substantially reduce the uncertainties on jet energy resulting from jet flavor. The presented m_t measurement is performed using the same data as Ref. [7], and is correlated with it as discussed below.

The D0 detector [12] is a multipurpose detector operated at the Fermilab Tevatron $p\bar{p}$ collider. The inner detector consists of coaxial cylinders and disks of silicon microstrips for track and vertex reconstruction. Eight layers of scintillating fibers arranged in doublets surround the silicon microstrip tracker and extend tracking measurements to forward pseudorapidities, η [13]. A 1.9 T solenoid produces a magnetic field for the tracking detectors. Uranium-liquid argon calorimeters surround the tracking volume and perform both electromagnetic and hadronic shower energy measurements. Thin scintillation intercryostat detectors sample showers in the region between the central and end calorimeters. Three layers of proportional drift tubes and scintillation counters reside outside the calorimetry, with 1.8 T toroids that provide muon identification and independent measurement of muon momenta.

We simulate $t\bar{t}$ events using Monte Carlo (MC) samples for 140 GeV $< m_t <$ 200 GeV using the ALPGEN generator [14] and PYTHIA [15] for parton fragmentation. Backgrounds originate from $Z/\gamma^* \to 2\ell$+jets and $WW/WZ/ZZ \to 2\ell$+jets production. For the former, we use ALPGEN combined with PYTHIA, while diboson backgrounds are simulated entirely with PYTHIA. We pass all MC events through a full detector simulation based on GEANT [16]. Backgrounds from instrumental effects that result in misidentified leptons are modeled using data.

We use single and two-lepton triggers to select events for this analysis. Data and simulated events are reconstructed to provide the momenta of tracks, jets, and lepton candidates. Charged leptons are required to be isolated from other calorimeter energy deposits, and to have an associated track in the inner detector. Calorimeter and tracking information are combined to identify electrons. Track parameters in the muon and inner detector system are used to identify muons. We reconstruct jets with an iterative, midpoint cone algorithm with radius $\mathcal{R}_{\rm cone} = 0.5$ [17]. Jets are calibrated with the standard D0 jet energy correction which is derived from data [18]. The method corrects the measured jet energy to the value obtained by applying the reconstruction cone algorithm to particles from jet fragmentation before they interact with the detector. We establish the efficacy of the method in the MC, where we compare the measured jet and the jet reconstructed from fragmentation particles. The jets in data and MC are calibrated independently so that their relative response is close to unity. This corrects for detector response, energy deposited outside of the jet cone, electronics noise, and pileup. The largest correction compensates for the detector response, and is extracted using γ+jet events in data and MC. We also correct jets for the p_T of any embedded muon and that of the associated neutrino. We initially apply this standard calibration [18] because it provides detailed p_T and η dependent corrections. It also provides distinct corrections to jets and the imbalance in event transverse momentum ($\not\!\!E_T$) because several components (e.g., noise and out-of-cone effects) result from the jet reconstruction algorithm rather than any undetected energy. In the p_T range of jets found in $t\bar{t}$ events, the uncertainty of the standard D0 jet energy calibration averages 2%, and is dominated by systematics. Because the flavor dependence of jet energy calibration can yield one of the largest systematic uncertainties on our measurement [4], we have improved our analysis by accounting for this dependence. We use responses of single particles from data and MC to determine the energy scale for different jet flavors. We correct MC jets by the ratio of data response to MC response according to their flavor to ensure that the MC reflects the flavor dependence in data, as in Ref. [10]. We calculate $\not\!\!E_T$ as the negative of the vector sum of all transverse components of calorimeter cell energies and muon track momenta, corrected for the response to electrons and jets.

Events are selected to have two leptons (ee, $e\mu$, $\mu\mu$) and two or more jets. The leptons must have $p_T >$ 15 GeV and the jets must have $p_T >$ 20 GeV. Electrons and jets are required to satisfy $|\eta| < 2.5$, while muons must have $|\eta| < 2$. We further require $\not\!\!E_T >$ 40 GeV in the $\mu\mu$ channel. The $e\mu$ events must satisfy $H_T >$ 120 GeV, where H_T is defined to be the sum of the p_Ts of jets and the leading lepton. In $\mu\mu$ and ee events, we also require $\not\!\!E_T$ to be significantly larger than typical values found in the distribution from Z boson events. These and all other selections are detailed in Ref. [19]. We observe 50, 198, and 84 events with expected background yields of 10.4, 28.1, and 31.0 events in the ee, $e\mu$, and $\mu\mu$ channels, respectively.

In ℓ+jets events, one W boson decays to two quarks that fragment to jets. The invariant mass of this jet pair can be used to improve the calibration for all jets in these events. Complications arise because the four jets in the ℓ+jets events can be incorrectly assigned to the initial four quarks. Energy from different partons is also mixed in the same jet due to a high jet multiplicity. Observed jet energies are also affected by color flow effects, which are different for the b-quark jets and for jets from the decay of color singlet W bosons. These attributes are specific to a particular event topology such as ℓ+jets. Nevertheless, a scale factor based on the dijet invariant mass that is correlated with m_W can be extracted. The most recent analysis of this kind by D0 used 2.6 fb^{-1} of data and obtained a calibration factor of $1.013 \pm 0.008\,(\text{stat})$ [10]. The uncertainty of 0.8% is smaller than that of the standard jet energy correction and will decrease with additional data. There are additional systematic effects on this energy scale that one must account for when applying it to b-quark jets in the ℓ+jets analysis. These also affect our analysis, and we similarly evaluate the flavor dependence and residual energy scale systematic uncertainties directly on the measured m_t to avoid double counting. These are quoted in Table II and discussed below. Beyond this, we have the possible difference between b-quark jets in dilepton events and b-quark jets in ℓ+jets events and the effect of using a calibration based on a subset of the total data, each of which we discuss now in detail.

The event topology is different in 2ℓ and ℓ+jets events. This has prevented significant progress in reducing the large standard jet energy scale uncertainties in dilepton analyses. To overcome this challenge and carry over the ℓ+jets calibration, we must account for the possibility that the energy scale of the b-quark jets in the two channels can differ. We calculate the energy scale, $R^{2\ell}$, for b-quark jets in the dilepton sample using responses for single particles that fall within the reconstructed jet cone. This is done by scaling single particle responses in MC to reproduce the energy response of jets in data [9], giving $R^{2\ell}_{\text{data}}$, and using particle responses from MC, giving $R^{2\ell}_{\text{MC}}$. We calculate the ratio of these two responses in the dilepton channel and the analogous ratio for b-quark jets in the ℓ+jets sample. The corresponding double ratio

$$\mathcal{R}^b_{2\ell}(p^b_T) = \frac{R^{2\ell}_{\text{data}}(p^b_T)/R^{2\ell}_{\text{MC}}(p^b_T)}{R^{\ell+\text{jets}}_{\text{data}}(p^b_T)/R^{\ell+\text{jets}}_{\text{MC}}(p^b_T)}, \qquad (1)$$

varies between 1.001 and 1.003 depending on b-quark jet p_T, p^b_T. The multiplicity of particles in b-quark jets in ℓ+jets events at the MC generator level is, after application of the offline jet algorithm, a few percent higher than in the dilepton sample, which is a sufficiently large difference to account for the observed value of $\mathcal{R}^b_{2\ell}$. We therefore take 0.3%, the maximum excursion of $\mathcal{R}^b_{2\ell}$ from unity, as a systematic uncertainty on carrying over the ℓ+jets scale to the jets in our dilepton sample. The ℓ+jets scale is applied as a direct correction to the standard calibration.

The jet energy scale calibration obtained in Ref. [10] is based on a subset of the data, and we must therefore estimate the effect of using the calibration on a larger data set. The instantaneous luminosity of the dilepton sample is higher on average. We reweight the distribution of the number of primary vertices in the ℓ+jets sample to match the distribution in the 4.3 fb^{-1} ℓ+jets data and recalculate the ℓ+jets energy scale. This produces a negligible effect. To account for a possible shift in the energy scale of the liquid argon calorimeter, we apply a correction derived from 4.3 fb^{-1} rather than 2.6 fb^{-1}, and this yields a 0.7% shift in jet energy scale. From these studies, we obtain a total uncertainty on the ℓ+jets energy scale as applied to our analysis as the sum in quadrature of the statistical uncertainty (0.8%), $\mathcal{R}^b_{2\ell}$ (0.3%), and the calorimeter calibration (0.7%). This yields a 1.1% uncertainty for applying the ℓ+jets energy scale.

The consequence of two neutrinos in dilepton events is an underconstrained kinematics. We employ the νWT technique to extract m_t [6] due to its weak sensitivity to the modeling details of $t\bar{t}$ events. We integrate over the η distributions predicted for both neutrinos, solve the event kinematics, and calculate $\not\!\!E_T$ from the neutrino momentum solutions. The expected neutrino η distribution in the dilepton channel is symmetric around η=0 and found to be well-described by a Gaussian distribution. The width of the distribution decreases gradually with increasing m_t (i.e., as the neutrinos become more central). Hence, we model the neutrino η distributions with a Gaussian probability distribution using a width parameterized as a linear function of m_t. Several more sophisticated parametrizations were tested, but provided negligible improvement in expected precision in pseudo-experiments. By comparing the calculated $\not\!\!E_T$ to the measured $\not\!\!E_T$ for each event, we calculate a weight for a given choice of m_t. For each neutrino rapidity sampling, we sum the weights calculated from all combinations of neutrino momentum solutions and jet assignments. We therefore arrive at a distribution of relative weight for a range of m_t for each event. We found in Ref. [4] that most of the statistical sensitivity to m_t is obtained from the first two moments of this weight distribution, the mean (μ_w) and RMS (σ_w). A coarse granularity of our sampling of the η distribution causes these moments to be unstable. To reduce this variation, we have increased the sampling for this integration by an order of magnitude relative to our previous analysis [4]. This improves the expected statistical uncertainty on m_t by 4%. Requiring the integral of this distribution to be nonzero excludes events with a measured $\not\!\!E_T$ that is incompatible with coming from neutrinos from $t\bar{t}$ decay. This introduces a small inefficiency for the $t\bar{t}$ signal and reduces

TABLE I. Parameters used to calibrate $m_t^{\rm fit}$ in the analysis of ee, $e\mu$, and $\mu\mu$ channels and their combination.

Channel	Slope	Offset [GeV]	Pull width
ee	0.976 ± 0.014	0.03 ± 0.16	1.01 ± 0.01
$e\mu$	0.973 ± 0.012	0.43 ± 0.14	1.03 ± 0.01
$\mu\mu$	1.038 ± 0.022	0.49 ± 0.23	1.06 ± 0.03

the background contamination in the final sample. Our final kinematically reconstructed data sample consists of 49, 190, and 80 events in the ee, $e\mu$, and $\mu\mu$ channels, respectively.

Probability distributions for μ_w and σ_w are constructed for background in each channel. Each background component is normalized to its expected event yield. We generate distributions of $t\bar{t}$ signal probability as a function of μ_w, σ_w, and m_t. We use a binning that provides the minimum expected statistical uncertainty, as checked in pseudoexperiments. We perform a binned maximum likelihood fit to the probability distributions, fixing the total signal and background yields expected in our data. The signal is normalized to the cross section calculated for $t\bar{t}$ production [20], evaluated at $m_t = 172.5$ GeV. For all measurements, we obtain a likelihood (L) vs m_t. We fit a parabola to the dependence of $-\ln L$ vs. m_t, and the fitted mass, $m_t^{\rm fit}$, is defined as the lowest point of the parabola. Point-to-point fluctuations mean that the initial placement of the window may result in an nonconvergent fit. We therefore iterate the fit around the current fit minimum. This results in a significant improvement in fitting efficiency, particularly in the dimuon channel. The final $-\ln L$ vs. m_t for data is shown in Fig. 1. The statistical uncertainty for each measurement is taken as the half-width of the parabola at 0.5 units in $-\ln L$ above the minimum at $m_t^{\rm fit}$.

The above procedure is followed for the extraction of m_t from data and is used to calibrate the result as follows. We construct pseudoexperiments from signal and background MC samples according to their expected yields and allow fluctuations in each such that the total equals the number of observed events. We perform 1000 pseudoexperiments for each channel, and measure $m_t^{\rm fit}$ in each. A linear fit of $m_t^{\rm fit}$ vs the input m_t provides a calibration for our method. We also calculate the pull width of the average estimated statistical uncertainty vs the rms of $m_t^{\rm fit}$ values. The resulting slopes, offsets, and pull widths are given in Table I. The $m_t^{\rm fit}$ and estimated statistical uncertainty are corrected with these parameters. We obtain a calibrated mass measurement for the 4.3 fb^{-1} sample in the ee, $e\mu$, and $\mu\mu$ channels.

The largest systematic uncertainties are associated with the jet calibration. We change the ℓ+jets energy scale factor by $\pm 1.1\%$, and perform our analysis to obtain a systematic uncertainty on m_t of 0.9 GeV. The result of the ℓ+jets analysis is a single scale factor averaged over all jet p_Ts that are utilized in the dijet mass,

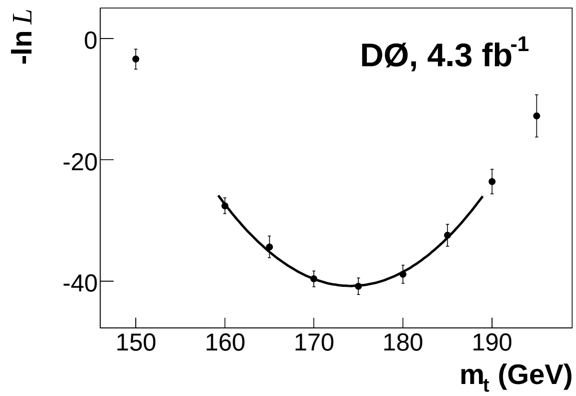

FIG. 1. -ln L as a function of m_t for the combined ee, $e\mu$, and $\mu\mu$ channels. A parabolic fit is shown near the minimum value in m_t.

i.e. dominated by light quark jets from W boson decay. As in Ref. [10], we estimate an uncertainty due to the difference in p_T distributions of b-quark jets, in our case in dilepton events, vs the calibrating jets from the $W \to jj$ sample. To estimate an uncertainty from this difference, we treat the p_T and η dependence of the uncertainty in the standard jet energy scale as a possible dependence of the residual energy scale following the calibration to ℓ+jets. We calculate the average of the energy scale uncertainty for jets in the $W \to jj$ sample. For each jet in the dilepton sample, we apply a shift corresponding to the difference between its uncertainty in energy scale and the $W \to jj$ sample's average uncertainty in energy scale. Propagating this difference through the mass analysis yields a 0.3 GeV uncertainty on m_t.

The flavor-dependent jet energy corrections described earlier provide MC-based mass templates that accurately reflect the data. As in [10], we propagate the uncertainty in these corrections and obtain a systematic uncertainty on m_t of 0.5 GeV. The uncertainties due to flavor dependence and residual scale together with the uncertainty originating from the carry over of the jet energy scale from the ℓ+jets sample account for the difference between b-quark jets in dilepton events and jets from $W \to jj$ in ℓ+jets events.

We evaluate the effect of our uncertainty in modeling initial state radiation (ISR) and final state radiation (FSR) by comparing two PYTHIA samples having identical values of generated m_t but different input parameters taken from a CDF study [21] corresponding to an increased or decreased amount of ISR/FSR. Color reconnection uncertainties are estimated by comparing the analysis with PYTHIA Tune Apro and PYTHIA Tune ACpro using [22]. Higher order QCD evolution is estimated by comparing ALPGEN configured with PYTHIA to MC@NLO with HERWIG [23] and this accounts for the uncertainty due to underlying event as well. To estimate sensitivity to uncertainties in the parton distribu-

TABLE II. Estimated systematic uncertainties on m_t for the combined dilepton measurement in 4.3 fb^{-1}.

Source	Uncertainty (GeV)
Jet energy calibration	
Overall scale	0.9
Flavor dependence	0.5
Residual scale	0.3
Signal modeling	
ISR/FSR	0.4
Color reconnection	0.5
Higher order effects	0.6
b quark fragmentation	0.1
PDF uncertainty	0.5
Object reconstruction	
Muon p_T resolution	0.2
Electron energy scale	0.2
Muon p_T scale	0.2
Jet resolution	0.3
Jet identification	0.3
Method	
Calibration	0.1
Template statistics	0.5
Signal fraction	0.2
Total systematic uncertainty	1.5

tion functions, we use CTEQ6M, and employ the method described in Ref. [24].

We modify the jet energy resolution in MC events to reflect the resolution in data. We evaluate the effect of an uncertainty in this procedure on the extraction of m_t by shifting the jet resolution by one standard deviation. We treat the electron and muon energy and momentum scales similarly and shift their calibrations within their uncertainties.

Pseudoexperiments are used similarly to account for the uncertainty in the method that arises from the uncertainties on the offset and slope in the calibration of the fitted m_t. We estimate the uncertainty due to the statistics employed in our templates of the $t\bar{t}$ probability distributions. We construct 1000 new templates, for both signal and background, and vary their bin contents within their Gaussian uncertainties. With these templates, we obtain 1000 new measurements from data and quote the rms of these values as a systematic uncertainty. We assign a systematic uncertainty on the signal fraction by shifting the background contributions in pseudoexperiments within their total uncertainty.

We combine measurements in the three dilepton channels using the method of "best linear unbiased estimator" [25]. We calculate each systematic uncertainty for the combined result, as given in Table II, according to its correlation among channels. The resulting measurement gives $m_t = 173.7 \pm 2.8\,(\text{stat}) \pm 1.5\,(\text{syst})$ GeV.

We combine this measurement with D0's measurement in the preceding 1 fb^{-1} of data using the νWT and matrix weighting methods [4]. Some uncertainties evaluated in the 4.3 fb^{-1} sample are not available for the 1.0 fb^{-1} sample. We include the new uncertainties in the result from the previous analysis. We consider statistical uncertainties, as well as the following systematic uncertainties to be uncorrelated: calibration of method, template statistics, overall jet energy scale, and flavor dependence. We consider all other uncertainties to be fully correlated. The combined measurement yields $m_t = 174.0 \pm 2.4\,(\text{stat}) \pm 1.4\,(\text{syst})$ GeV. This is consistent with measurements in other channels, and is the most precise single m_t measurement in the dilepton channel to date. We have also improved the precision by combining the νWT results with the results of Ref. [7]. The statistical correlation of these two measurements is approximately 60%, calculated from pseudoexperiments. Accounting for this correlation, and correlations appropriate to each source of systematic uncertainty, we obtain $m_t = 173.9 \pm 1.9\,(\text{stat}) \pm 1.6\,(\text{syst})$ GeV.

We thank the staffs at Fermilab and collaborating institutions, and acknowledge support from the DOE and NSF (USA); CEA and CNRS/IN2P3 (France); FASI, Rosatom and RFBR (Russia); CNPq, FAPERJ, FAPESP and FUNDUNESP (Brazil); DAE and DST (India); Colciencias (Colombia); CONACyT (Mexico); NRF (Korea); CONICET and UBACyT (Argentina); FOM (The Netherlands); STFC and the Royal Society (United Kingdom); MSMT and GACR (Czech Republic); BMBF and DFG (Germany); SFI (Ireland); The Swedish Research Council (Sweden); and CAS and CNSF (China).

[1] S. Chatrchyan *et. al.* (CMS Collaboration),Phys. Lett. B **716**, 30 (2012).
[2] G. Aad *et. al.* (ATLAS Collaboration),Phys. Lett. B **716**, 1 (2012).
[3] T.Aaltonen *et al.* (CDF Collaboration and D0 Collaboration), Phys. Rev. Lett. **109**, 071804 (2012).
[4] V. M. Abazov *et al.* (D0 Collaboration), Phys. Rev. D **80**, 092006 (2009).
[5] V. M. Abazov *et al.* (D0 Collaboration), Phys. Lett. B **655**, 7 (2007).
[6] S. Abachi *et al.* (D0 Collaboration), Phys. Rev. Lett. **80**, 2063 (1998).
[7] V. M. Abazov *et al.* (D0 Collaboration), Phys. Rev. Lett. **107**, 082004 (2011).
[8] V. M. Abazov *et al.* (D0 Collaboration), Nature **429**, 638 (2004).
[9] V. M. Abazov *et al.* (D0 Collaboration), Phys. Rev. D **85**, 052006 (2012).
[10] V. M. Abazov *et al.* (D0 Collaboration), Phys. Rev. D **84**, 032004 (2011).
[11] T. Aaltonen *et al.* (CDF Collaboration), Phys. Rev. D **83**, 111101 (2011).

[12] V. M. Abazov *et al.* (D0 Collaboration), Nucl. Instrum. Methods in Phys. Res. Sect. A **565**, 463 (2006); S. N. Ahmed *et al.*, Nucl. Instrum. Methods in Phys. Res. Sect. A **634**, 8 (2011); R. Angstadt *et al.*, Nucl. Instrum. Methods in Phys. Res. Sect. A **622**, 298 (2010); M. Abolins *et al.*, Nucl. Instrum. Methods in Phys. Res. Sect. A **584**, 75 (2008).

[13] The pseudorapidity is defined as $\eta = -\ln[\tan(\theta/2)]$ where θ is the polar angle relative to the beam axis, defined relative to the center of the detector.

[14] M. Mangano, F. Piccinini, A.D. Polosa, M. Moretti, and R. Pittau, J. High Energy Phys. **07**, 001 (2003); M. Mangano, M. Moretti and R. Pittau, Nucl. Phys. **B632**, 343 (2002); F. Caravaglios, M.L. Mangano, M. Moretti, and R. Pittau, Nucl. Phys. **B539**, 215 (1999).

[15] T. Sjöstrand *et al.*, Comput. Phys. Commun. **135**, 238 (2001).

[16] R. Brun and F. Carminati, CERN Program Library Long Writeup W5013, 1993 (unpublished).

[17] G. Blazey *et al.*, arXiv:hep-ex/0005012 (2000).

[18] V.M. Abazov *et al.* (D0 Collaboration), Phys. Rev. D **85**, 052006 (2012); S. Abachi *et al.* (D0 Collaboration), Nucl. Instrum. Methods in Phys. Res., Sect. A **424**, 352 (1999).

[19] V. M. Abazov *et al.* (D0 Collaboration), Phys. Lett. B **704**, 403 (2011).

[20] S. Moch and P. Uwer, Phys. Rev. D **78**, 034003 (2008).

[21] T. Aaltonen *et al.*, arXiv:1207.1069v2 [hep-ex] (2012).

[22] A. Buckley *et al.*, Eur. Phys. J. C **65**, 331 (2010); R. Field and R. C. Group, arXiv:hep-ph/0510198. The difference between the ACpro and Apro tunes is used to estimate the systematic uncertainty related to color reconnection.

[23] G. Corcella *et al.*, J. High Energy Phys. **01**, 010 (2001).

[24] J. Pumplin *et al.*, J. High Energy Phys. **07**, 012 (2002); D. Stump *et al.*, J. High Energy Phys. **10**, 046 (2003).

[25] L. Lyons, D. Gibaut, and P. Clifford, Nucl. Instrum. Methods Phys. Res. A **270**, 110 (1988); A. Valassi, Nucl. Instrum. Methods Phys. Res. A **500**, 391 (2003).